HHS Public Access

Author manuscript

J Am Chem Soc. Author manuscript; available in PMC 2021 February 05.

Published in final edited form as:

J Am Chem Soc. 2020 February 05; 142(5): 2244–2252. doi:10.1021/jacs.9b09070.

Molecular Basis for Spirocycle Formation in the Paraherquamide Biosynthetic Pathway

Amy E. Fraley[1,2], **Kersti Caddell Haatveit**[3], **Ying Ye**[1], **Samantha P. Kelly**[1,4], **Sean A. Newmister**[1], **Fengan Yu**[1], **Robert M. Williams**[5,6,*], **Janet L. Smith**[1,4,7,*], **K. N. Houk**[3,*], **David H. Sherman**[1,2,4,8,9,*]

[1]Life Sciences Institute, University of Michigan, Ann Arbor, Michigan 48109, USA

[2]Department of Medicinal Chemistry, University of Michigan, Ann Arbor, Michigan 48109, USA

[3]Department of Chemistry and Biochemistry, University of California, Los Angeles, California 90095, USA

[4]Program in Chemical Biology, University of Michigan, Ann Arbor, Michigan 48109, USA

[5]Department of Chemistry, Colorado State University, Fort Collins, Colorado 80523, USA

[6]University of Colorado Cancer Center, Aurora, Colorado 80045, USA

[7]Department of Biological Chemistry, University of Michigan, Ann Arbor, Michigan 48109, USA

[8]Department of Chemistry, University of Michigan, Ann Arbor, Michigan 48109, USA

[9]Department of Microbiology and Immunology, University of Michigan, Ann Arbor, Michigan 48109, USA

Abstract

The paraherquamides are potent anthelmintic natural products with complex heptacyclic scaffolds. One key feature of these molecules is the *spiro*-oxindole moiety that lends a strained three-dimensional architecture to these structures. The flavin monooxygenase PhqK was found to catalyze spirocycle formation through two parallel pathways in the biosynthesis of paraherquamides A and G. Two new paraherquamides (K and L) were isolated from a Δ*phqK* strain of *Penicillium simplicissimum*, and subsequent enzymatic reactions with these compounds generated two additional metabolites paraherquamides M and N. Crystal structures of PhqK in complex with various substrates provided a foundation for mechanistic analyses and computational studies. While it is evident that PhqK can react with various substrates, reaction kinetics and molecular dynamics simulations indicated that the dioxepin-containing paraherquamide L was the favored substrate. Through this effort, we have elucidated a key step in the biosynthesis of the paraherquamides, and provided a rationale for the selective spirocyclization of these powerful anthelmintic agents.

[*]**Corresponding Authors**: davidhs@umich.edu, houk@chem.ucla.edu, JanetSmith@umich.edu, Robert.Williams@colostate.edu.

Author Contributions

The manuscript was written through contributions of all authors. All authors have given approval to the final version of the manuscript.

Supporting Information

Full experimental details and computational methods, NMR spectra, tables, and figures.

PDB IDs: 6pvf, 6pvg, 6pvh, 6pvi, 6pvj

Graphical Abstract

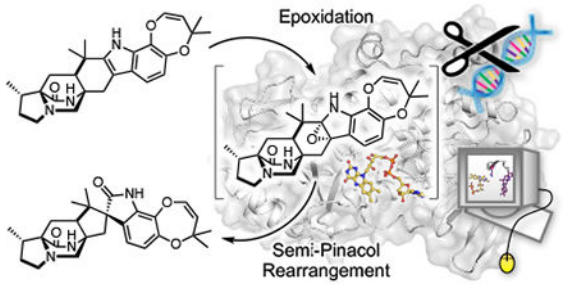

Keywords

spirocycle; biocatalysis; monooxygenase; flavin; alkaloid

INTRODUCTION

The paraherquamide family of natural products contains metabolites isolated from various species of *Penicillium* including *P. paraherquei*,[1] *P. charlesii*,[2] *P. cluniae*,[3] *P. fellutanum*,[4] and *P.* IMI 332995.[5] These molecules are of particular interest due to their anthelmintic therapeutic potential, and various analogs have been developed to improve their pharmacological properties.[6–9] Derquantel, or 2-deoxyparaherquamide A, is currently used in combination with the established anthelmintic abamectin to combat gastrointestinal nematode infections in sheep.[10] The significant biological activity of this family of molecules is complemented by the intriguing biosynthetic chemistry including intramolecular Diels-Alder cyclization, unusual oxidative substitutions, and *spiro*-oxindole formation.

Paraherquamide-type molecules belong to a family of fungal indole alkaloids containing a unique bicyclo[2.2.2]diazaoctane ring, which is formed through a [4+2] intramolecular Diels-Alder (IMDA) reaction.[11] The spirocycle is a common functionality of many molecules within this family including the marcfortines,[12, 13] brevianamides,[14, 15] antiinsectan sclerotiamide,[16] and cytotoxic notoamides.[17] The respective enzymes involved in spirocycle formation are proposed to generate an initial C2=C3 indole epoxide with facial selectivity, and controlled collapse of the epoxide giving rise to the observed *spiro*-oxindoles. Very few enzymes responsible for this type of reaction within the bicyclo-ring containing family have been characterized.[18] NotB catalyzes the 2,3-β-face epoxidation of notoamide E (**1**) to generate the non-*spiro*-cyclized terminal metabolites notoamides C (**2**) and D (**3**), which are not IMDA substrates. In this pathway, another flavin-dependent monooxygenase NotI performs a presumed 2,3-α-face epoxidation of stephacidin A (**4**) in the process of generating the bioactive natural product notoamide B (**5**) (Figure 1a). These flavin-dependent monooxygenases have evolved to perform facially selective epoxidation either before or after the IMDA cyclization, resulting in a divergence in the notoamide biosynthetic pathway.

Biocatalytic epoxidation typically occurs through reactions with molecular oxygen which is activated either by a metal ion or flavin adenine dinucleotide (FAD) cofactor.[19] The enzyme active site orients the substrate for facial selectivity of the epoxidation, and in some cases, subsequent collapse of the epoxide in a stereocontrolled manner to generate complex molecular structures (Figure 1b). Enantioselective oxidation is a common step in the syntheses of many natural products and bioactive molecules, including complex alkaloids.[20, 21] In particular, indole-2,3-epoxidation serves as a synthetic intermediate to rearrangements that generate a variety of products. The collapse of this intermediate can be directed by the inherent reactivity of the substrate or through a catalyst-controlled mechanism. For example, synthetic methods have been developed to favor spirocyclization[22–25] or other oxidized products[20] in the total syntheses of select fungal indole alkaloids.

While synthetic methods for enantioselective epoxidation and spirocyclization are rapidly improving, the role of biocatalysis for solving synthetic challenges is also gaining greater visibility. The inherent selectivity of enzymes is unparalleled in synthetic chemistry and with each enzymatic discovery, the biocatalytic toolbox is broadening. In particular, there is evidence that oxygenases can be successfully employed in the generation of enantiomerically pure starting materials for total syntheses.[27] To this end, a few enzymes that catalyze epoxidation and subsequent spirocyclization have been identified.

Of the currently characterized natural products that include *spiro*-centers, most structures fall outside of the bicyclo[2.2.2]diazaoctane ring-containing family, and the predicted biosynthetic enzymes utilize either metal-dependent radical-based mechanisms[28,29] or flavin-dependent redox chemistry (Figure 1).[30] In some cases, the spirocyclic scaffold is known to be critical for biological activity.[29] Studies detailing spirocycle formation in the spirotryprostatins revealed intricate enzymatic details for this conversion.[31] Two distinct routes for the formation of this spirocyclic moiety involve either a flavin monooxygenase (with homology to NotB[18]), which employs an indole epoxidation route to generate spirotryprostatin A (**6**), or a cytochrome P450 that involves a radical route to generate spirotryprostatin G (**7**), both starting from fumitremorgin C (**8**). Cross talk between the flavin-dependent monooxygenase from the fumiquinazoline biosynthetic pathway and enzymes from the fumitremorgin biosynthetic pathway have led to the generation of unique diketopiperazine-containing spirocyclic metabolites in *Aspergillus fumigatus*. While these functional studies provided important insights regarding the various mechanisms of formation for the spirocyclized natural products, stmctural data for the key biocatalysts has remained elusive.

The paraherquamide class of natural products contains a *spiro*-oxindole center within a complex heptacyclic ring system. The biosynthesis of these molecules starts with the condensation of L-tryptophan and L-β-methyl-proline,[32–34] followed by spontaneous oxidation to generate zwitterion **9** (Scheme 1).[35, 36] Reverse prenylation at the indole C2 position provides the prenylated zwitterion substrate **10**, which is reduced to azadiene **11** and cyclized by the Diels-Alderase[11] to produce preparaherquamide (**12**). While precursor incorporation studies demonstrated that **12** is incorporated into the final product (−)-paraherquamide A (**13**),[36] it was unclear whether the spirocyclization occurred before or

after the formation of the pyran and dioxepin rings. Through disruption of *phqK* in *Penicillium simplicissimum* using a CRISPR-Cas9 system, we identified that **12** undergoes a series of oxidation and prenylation reactions to generate paraherquamides K and L (**14** and **15**) prior to *spiro*-cyclization by PhqK.[4, 35, 36] This enzyme was characterized *in vitro* as a flavin-dependent monooxygenase, which acts on native substrates **14** and **15** to generate the corresponding spirocyclized products. Crystal structures of PhqK in complex with its native substrates revealed precise substrate orientation to promote selective epoxidation thereby enabling stereospecific formation of the *spiro*-oxindole moiety.

Consistent with previous hypotheses, we have proposed a mechanism based on indole α-epoxidation and collapse of the putative epoxide at C3 to generate a C2 hydroxyl carbocation.[26] Subsequent migration of the reverse prenyl group from C2 to C3 would generate the 2-oxindole product. The work described here provides the first structural data for this unique class of spirocycle forming flavin monooxygenases, and sheds light on biocatalytic control of epoxide formation and mode of Pinacol rearrangement.

RESULTS

Parallel efforts were pursued *in vitro* and *in vivo* to identify the enzyme responsible for the spirocyclization reaction in paraherquamide biosynthesis. Paraherquamide K (**14**) and paraherquamide L (**15**) accumulated from the Δ*phqK* strain of *Penicillium simplicissimum* (Supplemental Figures 32 and 33), indicating that both molecules are natural substrates of the enzyme. The *in vitro* reactions of **14** and **15** with PhqK confirmed their conversion into the respective spirocyclized products paraherquamide M (**16**) and paraherquamide N (**17**). This information provided evidence to support a branched biosynthetic scheme where the pyran and dioxepin rings are both formed prior to the spirocyclization (Scheme 1). The identification of two natural substrates for PhqK indicates that functionalization of **12** is the divergent step between two parallel pathways leading to paraherquamides G (**18**) and A (**13**). In the first case, a putative prenyltransferase and oxidative enzyme build the pyran ring, whereas the latter involves generation of the dioxepin ring by a poorly understood process.[35] PhqK accepts both substrates, thus the downstream *N*-methyltransferase and β-methyl proline hydroxylase must also display the same level of substrate flexibility.

To obtain further information about the selectivity of PhqK, we employed Michaelis-Menten kinetic analysis (Supplemental Figures 34 and 35). Although the pyran-containing **14** displayed a higher turnover number (k_{cat}), the K_m for **15** (19.4 ± 5.2 μM) was significantly lower compared to **14** (92.1 ± 29.4 μM). This resulted in nearly equivalent catalytic efficiencies (k_{cat}/K_m) for both substrates (0.05 ± 0.01 $\mu M^{-1}min^{-1}$ for **15** and 0.04 ± 0.01 $\mu M^{-1}min^{-1}$ for **14**), however based on the low probability that these secondary metabolites are present at saturating concentrations *in vivo*, we reasoned that **15** is likely the favored substrate.

The high yields and activity of PhqK indicated its potential as a biocatalyst, thus the substrate scope was analyzed on a series of structurally related malbrancheamide analogs. The halogenated malbrancheamides are produced by two fungal species, including the terrestrial strain *Malbranchea aurantiaca*[37] and the marine-derived *Malbranchea graminicola*.

[38] The corresponding biosynthetic gene clusters for malbrancheamide (**19**) and spiromalbramide (**20**) from these two fungi possess 99% amino acid sequence identity.[39] Intriguingly, the spirocyclized malbrancheamide analog spiromalbramide has only been isolated from the marine fungus.[38] Therefore, we tested the reactivity of PhqK on the halogenated malbrancheamide and analogs malbrancheamides B (**21**), C (**22**), E (**23**), and isomalbrancheamide D (24).[39] The reactions generated a variety of spirocyclized malbrancheamides (**20**, **25**-**28**) including the natural product spiromalbramide (**20**), indicating that a PhqK homolog in *M. graminicola* may be involved in spiromalbramide biosynthesis (Figure 2, Supplemental Figures 11–31, and Supplemental Tables 7–16).[38] PhqK catalyzes formation of products with a relative stereochemical outcome matching that identified in the natural metabolites (5a*R*, 6a*S*, 12a*S*, 13a*S*) and demonstrated its ability to accept non-native substrates such as the malbrancheamides. While efficient conversion of the malbrancheamides was achieved, the conversion of smaller, less structurally complex substrates was not observed (Figures S47–S49). This indicates an evolutionary distinction between early- and late-stage Pinacolase enzymes, as previously demonstrated in the notoamide biosynthetic pathway.[18]

In an effort to improve the efficiency of PhqK, we analyzed reactions in the presence of a cofactor regeneration system (glucose-6-phosphate dehydrogenase) and catalase to eliminate the detrimental effects of hydrogen peroxide resulting from the flavin redox chemistry. In the presence of stoichiometric FAD concentrations, the use of the regeneration system (Figure S45) and catalase (Figure S44) significantly increased the conversion of non-native substrates, while conversions of **14** and **15** remained unaffected (Figures S40–S43). This system may mimic the enzyme's natural environment in the producing organism, and we expect that with the aid of other enzymes commonly found in fungi, PhqK may be more efficient.

With this foundational knowledge, we proceeded to elucidate the molecular basis for stereospecificity by analyzing the structure of the enzyme. PhqK was cocrystallized as four distinct substrate complexes, bearing the natural pyran-containing **14** (1.89 Å) and dioxepin-containing **15** (2.09 Å), and non-native substrates monochlorinated malbrancheamide B (**21**) (1.69 Å), and monobrominated malbrancheamide C (**22**) (1.25 Å). A ligand-free structure was also obtained (1.71 Å), aiding the visualization of how the active site changes to accommodate the hexa- and heptacyclic alkaloids (Figure 3). The FAD binding pocket and substrate binding pocket are connected by a long tunnel that appears to put significant distance between the cofactor and the substrate. This can be explained by the well-characterized flavin dynamics described in previous work.[40,41] Flavin monooxygenases commonly display a dynamic cofactor with an orientation that is dependent on discrete parameters, including substrate binding or cofactor oxidation state. In both substrate bound and unbound PhqK structures, the flavin was observed in the "out" conformation. It is hypothesized that the "in" conformation may be induced by reduction of the FAD cofactor, but our attempts to obtain a structure bound to reduced flavin using sodium dithionite and NADH were unsuccessful. As an alternative, we modelled the "in" conformation of the cofactor from HpxO[42] into the PhqK structure (Figures 4 and 5). HpxO is a FAD-dependent urate oxidase from *Klebsiella pneumoniae* and its secondary structure overlays well with

PhqK (26% sequence identity, RMSD 1.54 Å), with the major differences attributed to FAD conformation. Divergence in the FAD monooxygenase family is based on evolutionary domain fusion events leading to differences in the substrate binding pocket and reactivity,[43] thus this structural similarity in the cofactor binding region is expected.

When inspecting the overlay of PhqK with HpxO, we observed that the main changes are localized to the substratebinding region where two loops, one near the cofactor and one near the substrate, are altered in HpxO. Whereas the FAD cofactor in the PhqK structure reveals the “out” position, the FAD in HpxO is found as the “in” position, making it a suitable model for generating a visual representation of this phenomenon in PhqK. The “in” flavin from HpxO was modelled into the PhqK structure and fit well in the active site tunnel. In this orientation, the C4a-OOH-FAD would reside sufficiently close to the substrate (6.5 Å between C4a and indole C2/C3) to catalyze epoxidation at the indole C2=C3 position (Figures 4 and 5). Inspection of the substrates in PhqK structural complexes revealed that each one binds in the same manner except for **15**, which is oriented for direct α-epoxidation. It is possible that the individual substrates sample both conformations in solution. Since **15** appears to be the favored substrate, it may preferentially bind in the active conformation, explaining performed 1,500 ns MD simulations which demonstrated that **15** maintains a more rigid binding pose with better facial selectivity for epoxidation. By contrast, **14** is more flexible within the binding pocket and adopts less productive conformations for epoxidation (Supplemental Figure 54). Site-directed mutagenesis experiments revealed the importance of specific amino acid residues in the active site. Most of the mutants led to significant losses in flavin incorporation within the protein (indicated as %FAD in Supplemental Table 17) and a decrease in enzyme stability (indicated as [PhqK] in Supplemental Table 17). Mutation of certain active site residues abolished enzyme activity, indicating that they may perform essential catalytic roles. For example, Gln232, which interacts with the indole N-H, is necessary for conversion of both **14** and **15** to the corresponding *spiro*-oxindole forms. Substitutions of alanine and glutamate at this site abrogated catalytic activity toward **15**, while **14** exhibited about 2% conversion. Additionally, Arg192 and Asp47 are two essential amino acid residues within the tunnel between the substrate and cofactor. When Arg192 was substituted with alanine and lysine, **15** was not converted to product, while **14** showed 5-10% conversion.

The substitutions of alanine and asparagine for Asp47 also led to a complete loss of activity. All of these residues are located on the indole N-H side of the substrate and thus could play a role in directing the collapse of the epoxide and why we captured that pose in the crystal structure. We semi-Pinacol rearrangement to this side of the molecule. Arg192 clashes with the modeled “in” flavin, indicating that it must move in concert with the swing of the cofactor. We hypothesize that Arg192 moves closer to the substrate upon epoxidation and can serve as a general acid to catalyze epoxide opening (Figure 6). The distance between Arg192 and the indole C2 is around 7 Å. With a full extension of Arg192, it would be close enough to the substrate to facilitate general acid catalysis (Figure 6 and Scheme 2). An analysis of Arg192 using PROPKA on the PDB2PQR server[44] indicated that the pK_a of this general acid decreased as the conformation of the enzyme approached the catalytically competent pose (Table S20). The well-established conformational flexibility of arginine and

dynamics of these flavin-dependent enzymes are indicative of a drastic change in the active site during catalysis. As we observed the pK_a value decreasing upon binding **15** in a more catalytically competent pose, we hypothesize that once the FAD cofactor moves to the "in" position, the environment of this hydrophobic pocket would be adequate for lowering the pK_a of Arg192 for the protonation event.

Next, we performed density functional theory (DFT) calculations to explore different mechanisms and indole substituent effects on epoxide ring opening for the generation of the *spiro*-oxindole products. Our calculations involved the truncated indole fragment **29**, as a model substrate with varying methoxy substitutions to model the electronic effects of substrates **14** and **15** (Scheme 2). Under general acid catalysis by Arg192 (modelled by a guanidinium moiety), the epoxide opening step in Route 1 is preferred over Route 2 when there is a C6 methoxy substituent due to the additional electronic stabilization of C2 hydroxyl carbocation **31**, whereas in the alternative pathway C3 hydroxyl carbocation **34** does not benefit from this stabilization.

While this substitution plays a role, the subsequent carbon bond migration is the rate-limiting step. We evaluated the effect of the general acid and the indole substitutions on the Gibbs energy of the transition state (Figure 7). The general acid, Arg192, significantly lowers the barrier by 6.5 kcal/mol for Route 1 and 3.9 kcal/mol for Route 2. While both Routes 1 and 2 have lower barriers, Route 1 always has a lower transition state Gibbs energy regardless of the substitution pattern due to the ground state stabilization of C3 hydroxyl carbocation **34** in Route 2. This indicates that the formation of the experimentally observed *spiro*-oxindoles is intrinsically preferred and PhqK lowers the transition state energy for this 1,2 shift through a general acid catalyzed mechanism.

DISCUSSION

The *spiro*-oxindole moiety occurs in a variety of natural products and its biosynthesis is of significant interest due to the therapeutic potential of these metabolites.[29] The spirocyclic scaffold has increasingly been utilized in the drug development process due to its unique structural attributes.[45] Additionally , the chemistry of the reaction is intriguing from a biochemical standpoint due to the numerous factors contributing to the selectivity. A variety of enzymes have been found to catalyze spirocycle forming reactions including copper-dependent oxidases, cytochromes P450, and FAD-dependent monooxygenases. In the metal-dependent enzymes, the reaction is proposed to proceed through a radical-based mechanism, while the flavin-dependent enzymes proceed through FAD redox chemistry.

We have characterized the FAD-dependent monooxygenase PhqK as the spirocycle generating enzyme within the paraherquamide biosynthetic pathway. Through elucidation of this key step, we have developed a revised biosynthetic scheme for the production of paraherquamides A and G in which spirocyclization occurs after formation of the pyran and dioxepin moieties. We demonstrated that PhqK accepts both **14** and **15**, confirming the existence of two parallel pathways (branching from **12**) within the paraherquamide-producing *Penicillium* strains. While both substrates are accepted by the enzyme, the kinetic data and molecular dynamics simulations indicate that **15**, bearing the dioxepin, is likely the

favored substrate *in vivo*. This provides evidence that the difference in the orientation of **15** observed in the PhqK cocrystal structure is due to its persistence in the catalytically competent pose, whereas the less favored substrates might occupy a resting state until the flavin redox chemistry is initiated. The orientation of the molecule within the active site sets selectivity for α-epoxidation as demonstrated by the **15**-bound structure.

Moreover, directed collapse of the initial 2,3-indole epoxide is likely mediated through general acid catalysis via Arg192 and has an energetic preference for migration of the prenyl group to C3 with oxidation at C2 of the indole. This is in excellent agreement with results from a similar system in the brevianamide family where the authors observed exclusive formation of the indoxyl product **36** resulting from the C3 hydroxyl carbocation.[45] From DFT calculations, they concluded that the enzyme should favor a general base mechanism via a glutamate residue. This makes the transition state barrier lower for the 1,2 shift involving the C3 hydroxyl intermediate **34**, over the general acid mechanism which favors the product from C2 hydroxyl intermediate **31**. These results indicate that stereocontrol of the *spiro*-oxindole product results from the mechanistic mode dictated by the particular enzyme rather than a substituent effect on the indole ring.

The current study has provided new insights into the structure and mechanism of flavin-dependent spirocycle-generating enzymes, and the evidence supports a selective epoxidation of the indole C2=C3 followed by a stereoselective collapse of the epoxide. While PhqK catalyzes spirocyclization at a late-stage in paraherquamide biosynthesis, homologous enzymes within the brevianamide, notoamide, and other indole alkaloid pathways can generate Pinacol-rearrangement products with varying stereochemistry, or bearing non-spirocyclic functionality. Some of these transformations even require multiple enzymes, while PhqK operates as a dual function oxidase/Pinacolase to generate the spirocyclized paraherquamides.

Supplementary Material

Refer to Web version on PubMed Central for supplementary material.

ACKNOWLEDGMENTS

The authors thank the National Institutes of Health for financial support, including R01 CA070375 to R.M.W. and D.H.S., R35 GM118101 and the Hans W. Vahlteich Professorship to D.H.S., R01 GM124480 to K.N.H., R01 DK042303 and the Margaret J. Hunter Professorship to J.L.S., The Rackham Predoctoral Fellowship to A.E.F., and NIH Predoctoral Training Grant GM067555 to K.C.H. GM/CA@APS is supported by the National Institutes of Health, National Institute of General Medical Sciences (AGM-12006) and National Cancer Institute (ACB-12002). The Advanced Photon Source is a U.S. Department of Energy (DOE) Office of Science User Facility operated by Argonne National Laboratory under Contract DE-AC02-06CH11357. Computational resources were provided by the UCLA Institute for Digital Research and Education (IDRE) and the Extreme Science and Engineering Discovery Environment (XSEDE), which is supported by the NSF (OCI-1 053575). The authors also thank Rajani Arora, UM LSI Multimedia and Social Media Specialist, for contributions in preparation of the Supplemental cover art.

REFERENCES

1. Yamazaki M; Okuyama E; Kobayashi M; Inoue H, The structure of paraherquamide, a toxic metabolite from *Penicillium paraherquei*. Tetrahedron Lett 1981, 22 (2), 135–136.

2. Ondeyka JG; Goegelman RT; Schaeffer JM; Kelemen L; Zitano L, Novel antinematodal and antiparasitic agents from *Penicillium charlesii* 1. Fermentation, isolation and biological activity. J Antibiot 1990, 43 (11), 1375–1379. [PubMed: 2272914]

3. López-Gresa MP; González MC; Ciavatta L; Ayala I; Moya P; Primo J, Insecticidal activity of paraherquamides, including paraherquamide H and paraherquamide I, two new alkaloids isolated from *Penicillium cluniae*. J Agr Food Chem 2006, 54 (8), 2921–2925. [PubMed: 16608209]

4. Sommer K; Williams RM, Studies on paraherquamide biosynthesis: synthesis of deuterium-labeled 7-hydroxy-preparaherquamide, a putative precursor of paraherquamides A, E, and F. Tetrahedron 2009, 65 (16), 3246–3260. [PubMed: 20161298]

5. Blanchflower SE; Banks RM; Everett JR; Reading C, Further novel metabolites of the paraherquamide family. J Antibiot 1993, 46 (9), 1355–1363. [PubMed: 8226314]

6. Blizzard TA; Margiatto G; Mrozik H; Schaeffer JM; Fisher MH, Chemical modification of paraherquamide 3. Vinyl ether modified analogs. Tetrahedron Lett 1991, 32 (22), 2437–2440.

7. Blizzard TA; Marino G; Mrozik H; Fisher MH; Hoogsteen K; Springer JP, Chemical modification of paraherquamide 1. Unusual reactions and absolute stereochemistry. J Org Chem 1989, 54 (11), 2657–2663.

8. Blizzard TA; Mrozik H; Fisher MH; Schaeffer JM, Chemical modification of paraherquamide 2. Replacement of the C-14 methyl group. J Org Chem 1990, 55 (7), 2256–2259.

9. Blizzard TA; Margiatto G; Mrozik H; Schaeffer JM; Fisher MH, Chemical modification of paraherquamide 4. 1-N-Substituted analogs. Tetrahedron Lett 1991, 32 (22), 2441–2444.

10. Little PR; Hodge A; Watson TG; Seed JA; Maeder SJ, Field efficacy and safety of an oral formulation of the novel combination anthelmintic, derquantel-abamectin, in sheep in New Zealand. New Zeal Vet J 2010, 58 (3), 121–129.

11. Dan Q; Newmister SA; Klas KR; Fraley AE; A. MT; Somoza AD; Sunderhaus JD; Ye Y; Shende VV; Yu F; Sander JN; Brown WC; Zhao L; Paton RS; Houk KN; Smith JL; Sherman DH; Williams RM, Fungal indole alkaloid biogenesis through evolution of a bifunctional reductase/Diels-Alderase. Nat Chem 2019, 11, 972–980. [PubMed: 31548667]

12. Polonsky J; Merrien MA; Prange T; Pascard C; Moreau S, Isolation and structure (X-ray analysis) of marcfortine A, a new alkaloid from *Penicillium roqueforti*. J.C.S. Chem. Comm 1980, 601–602.

13. Prangé T; Billion MA; Vuilhorgne M; Pascard C; Polonsky J; Moreau S, Structures of marcfortine B and marcfortine C (X-ray analysis), alkaloids from *Penicillium roqueforti*. Tetrahedron Lett 1981, 22 (21), 1977–1980.

14. Birch AJ; Wright JJ, Brevianamides - a new class of fungal alkaloid. Chem Commun 1969, (12), 644–645.

15. Birch AJ; Wright JJ, Studies in relation to biosynthesis. XLII. Structural elucidation and some aspects of biosynthesis of brevianamides A and brevianamides E. Tetrahedron 1970, 26 (10), 2329–3244. [PubMed: 5419195]

16. Whyte AC; Gloer JB, Sclerotiamide: a new member of the paraherquamide class with potent antiinsectan activity from the sclerotia of *Aspergillus sclerotiorum*. J Nat Prod 1996, 59 (11), 1093–1095. [PubMed: 8946752]

17. Kato H; Yoshida T; Tokue T; Nojiri Y; Hirota H; Ohta T; Williams RM; Tsukamoto S, Notoamides A-D: Prenylated indole alkaloids isolated from a marine-derived fungus, *Aspergillus* sp. Angew Chem Int Edit 2007, 46 (13), 2254–2256.

18. Li SY; Finefield JM; Sunderhaus JD; McAfoos TJ; Williams RM; Sherman DH, Biochemical characterization of NotB as an FAD-dependent oxidase in the biosynthesis of notoamide indole alkaloids. J Am Chem Soc 2012, 134 (2), 788–791. [PubMed: 22188465]

19. Grüschow S; Sherman DH, The biosynthesis of epoxides In Aziridines and epoxides in organic synthesis, Yudin AK, Ed. Wiley-VCH Verlag GmbH & Co. KGaA: Weinheim, 2006; pp 349–398.

20. Kolundzic F; Noshi MN; Tjandra M; Movaddaghi M; Miller SJ, Chemoselective and enantioselective oxidation of indoles employing aspartyl peptide catalysts. J. Am. Chem. Soc 2011, 133 (23), 9104–9111. [PubMed: 21539386]

21. Han L; Zhang W; Shi XX; You SL, Dearomatization of indoles via a phenol-directed vanadium-catalyzed asymmetric epoxidation and ring-opening cascade. Adv. Synth. Catal 2015, 357, 3064–3068.

22. Mercado-Marin EV; Garcia-Reynaga P; Romminger S; Pimenta EF; Romney DK; Lodewyk MW; Williams DE; Anderson RJ; Miller SJ; Tantillo DJ; Berlinck RGS; Sarpong R, Total synthesis and isolation of citrinalin and cyclopiamine congeners. Nature 2014, 509 (7500), 318–324. [PubMed: 24828190]

23. Artman GD; Grubbs AW; Williams RM, Concise, asymmetric, stereocontrolled total synthesis of stephacidins A, B and notoamide B. J Am Chem Soc 2007, 129 (19), 6336–6342. [PubMed: 17455936]

24. Greshock TJ; Grubbs AW; Jiao P; Wicklow DT; Gloer JB; Williams RM, Isolation, structure elucidation, and biomimetic total synthesis of versicolamide B, and the isolation of antipodal (−)-stephacidin A and (+)-notoamide B from *Aspergillus versicolor* NRRL 35600. Angew Chem Int Edit 2008, 47 (19), 3573–3577.

25. Greshock TJ; Grubbs AW; Tsukamoto S; Williams RM, A concise, biomimetic total synthesis of stephacidin A and notoamide B. Angew Chem Int Edit 2007, 46 (13), 2262–2265.

26. Grubbs AW; Artman GD; Tsukamoto S; Williams RM, A concise total synthesis of the notoamides C and D. Angew Chem Int Edit 2007, 46 (13), 2257–2261.

27. Faber K; Orru RVA, In Enzyme catalysis in organic chemistry, 2nd ed.; Drauz K; Waldmann H, Eds. Wiley-VCH: Weinheim, 2002; Vol. II, pp 579–608.

28. Huang KX; Fujii I; Ebizuka Y; Gomi K; Sankawa U, Molecular cloning and heterologous expression of the gene encoding dihydrogeodin oxidase, a multicopper blue enzyme from *Aspergillus terreus*. J Biol Chem 1995, 270 (37), 21495–21502. [PubMed: 7665560]

29. Cacho RA; Chooi YH; Zhou H; Tang Y, Complexity generation in fungal polyketide biosynthesis: A spirocycleforming P450 in the concise pathway to the antifungal drug griseofulvin. Acs Chem Biol 2013, 8 (10), 2322–2330. [PubMed: 23978092]

30. Ames BD; Haynes SW; Gao X; Evans BS; Kelleher NL; Tang Y; Walsh CT, Complexity generation in fungal peptidyl alkaloid biosynthesis: Oxidation of fumiquinazoline A to the heptacyclic hemiaminal fumiquinazoline C by the flavoenzyme Af12070 from *Aspergillus fumigatus*. Biochemistry 2011, 50 (40), 8756–8769. [PubMed: 21899262]

31. Tsunematsu Y; Ishikawa N; Wakana D; Goda Y; Noguchi H; Moriya H; Hotta K; Watanabe K, Distinct mechanisms for spiro-carbon formation reveal biosynthetic pathway crosstalk. Nat Chem Biol 2013, 9 (12), 818–825. [PubMed: 24121553]

32. Stocking EM; Sanz-Cervera JF; Williams RM; Unkefer CJ, Studies on the biosynthesis of paraherquamide A. Origin of the beta-methylproline ring. J Am Chem Soc 1996, 118 (29), 7008–7009.

33. Stocking EM; Martinez RA; Silks LA; Sanz-Cervera JF; Williams RM, Studies on the biosynthesis of paraherquamide: Concerning the mechanism of the oxidative cyclization of L-isoleucine to beta-methylproline. J Am Chem Soc 2001, 123 (14), 3391–3392. [PubMed: 11457085]

34. Stocking EM; Sanz-Cervera JF; Unkefer CJ; Williams RM, Studies on the biosynthesis of paraherquamide. Construction of the amino acid framework. Tetrahedron 2001, 57 (25), 5303–5320.

35. Stocking EM; Williams RM; Sanz-Cervera JF, Reverse prenyl transferases exhibit poor facial discrimination in the biosynthesis of paraherquamide A, brevianamide A, and austamide. J Am Chem Soc 2000, 122 (38), 9089–9098.

36. Stocking EM; Sanz-Cervera JF; Williams RM, Studies on the biosynthesis of paraherquamide: Synthesis and incorporation of a hexacyclic indole derivative as an advanced metabolite. Angew Chem Int Edit 2001, 40 (7), 1296–1298.

37. Martínez-Luis S; Rodríguez R; Acevedo L; González MC; Lira-Rocha A; Mata R, Malbrancheamide, a new calmodulin inhibitor from the fungus *Malbranchea aurantiaca*. Tetrahedron 2006, 62 (8), 1817–1822.

38. Watts KR; Loveridge ST; Tenney K; Media J; Valeriote FA; Crews P, Utilizing DART mass spectrometry to pinpoint halogenated metabolites from a marine invertebratederived fungus. J Org Chem 2011, 76 (15), 6201–6208. [PubMed: 21682275]

39. Fraley AE; Garcia-Borrás M; Tripathi A; Khare D; Mercado-Marin EV; Tran H; Dan Q; Webb GP; Watts KR; Crews P; Sarpong R; Williams RM; Smith JL; Houk KN; Sherman DH, Function and

structure of MalA/MalA', iterative halogenases for late-stage C-H functionalization of indole alkaloids. J Am Chem Soc 2017, 139 (34), 12060–12068. [PubMed: 28777910]

40. Ballou DP; Entsch B; Cole LJ, Dynamics involved in catalysis by single-component and two-component flavin-dependent aromatic hydroxylases. Biochem Bioph Res Co 2005, 338 (1), 590–598.
41. Entsch B; Cole LJ; Ballou DP, Protein dynamics and electrostatics in the function of p-hydroxybenzoate hydroxylase. Archives of Biochemistry and Biophysics 2005, 433, 297–311. [PubMed: 15581585]
42. Hicks KA; O'Leary SE; Begley TP; Ealick SE, Structural and mechanistic studies of HpxO, a novel flavin adenine dinucleotide-dependent urate oxidase from *Klebsiella pneumoniae*. Biochemistry 2013, 52 (3), 477–487. [PubMed: 23259842]
43. Mascotti ML; Ayub MJ; Furnham N; Thornton JM; Laskowski RA, Chopping and changing: the evolution of the flavin-dependent monooxygenases. J Mol Biol 2016, 428 (15), 3131–3146. [PubMed: 27423402]
44. Dolinksy TJ; Nielsen JE; McCammon JA; Baker NA PDB2PQR: an automated pipeline for the setup of Poisson-Boltzmann electrostatics calculations. Nucleic Acids Res. 2004 32, W665–W667. [PubMed: 15215472]
45. Zheng YJ; Tice CM; Singh SB, The use of spirocyclic scaffolds in drug discovery. Bioorganic & Medicinal Chemistry Letters 2014, 24 (16), 3673–3682. [PubMed: 25052427]
46. Ye Y; Du L; Zhang X; Newmister SA; Zhang W; Mu S; Minami A; McCauley M; Alegre-Requena JV; Fraley AE; Androver-Castellano ML; Shende VV; Oikawa H; Kato H; Tsukamoto S; Paton R; Williams RM; Sherman DH; Li S, Cofactor-independent Pinacolase directs non-Diels-Alderase biogenesis of the brevianamides. ChemRxiv 2019 10.2634/chemrxiv.9122009.v1

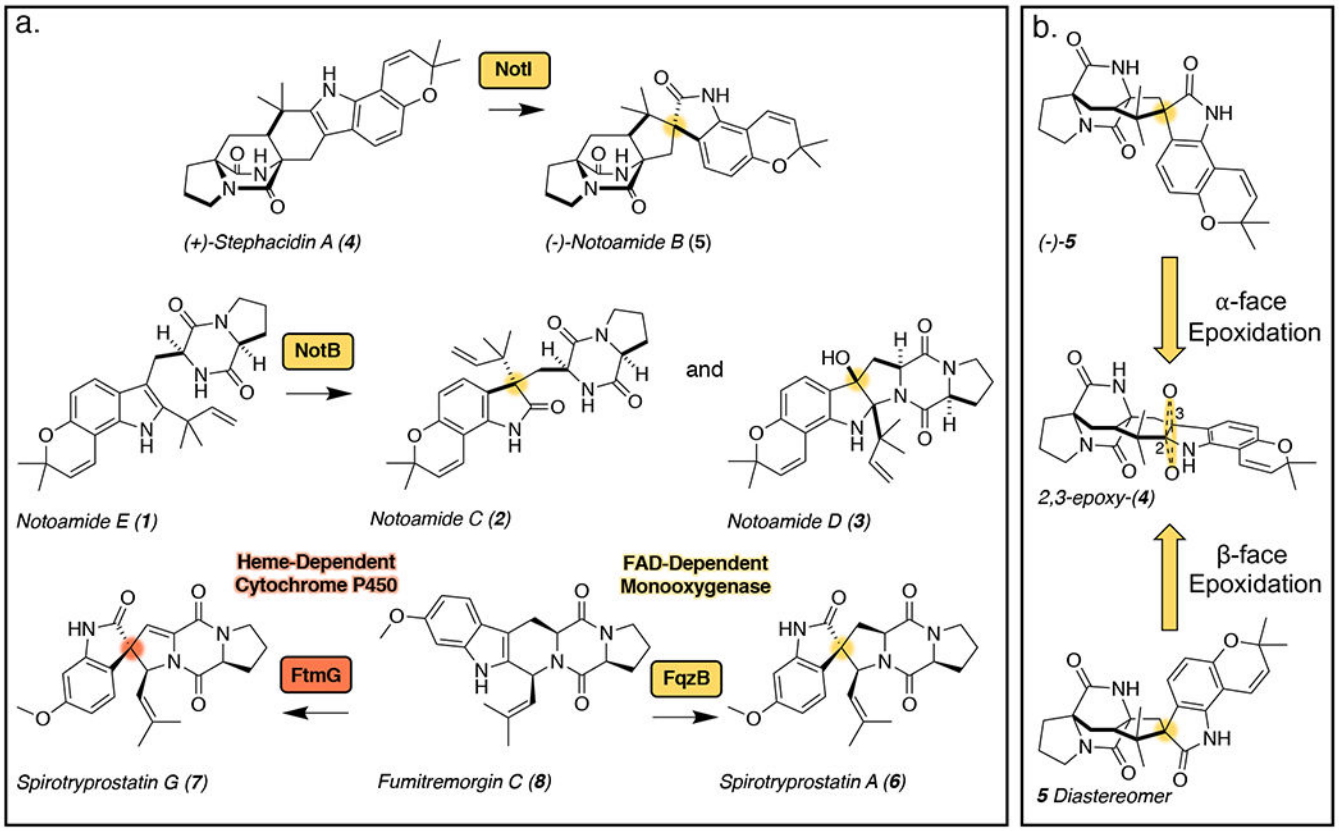

Figure 1.

(a.) Indole alkaloid products resulting from the various enzyme selectivities for the indole epoxide collapse. (b.) Representation of the biocatalyst-controlled facial selectivity of the presumed epoxidation of stephacidin A (**4**) to generate (−)-notoamide B (**5**) through α-face epoxidation and the unnatural diastereomer of **5** through β-face epoxidation.

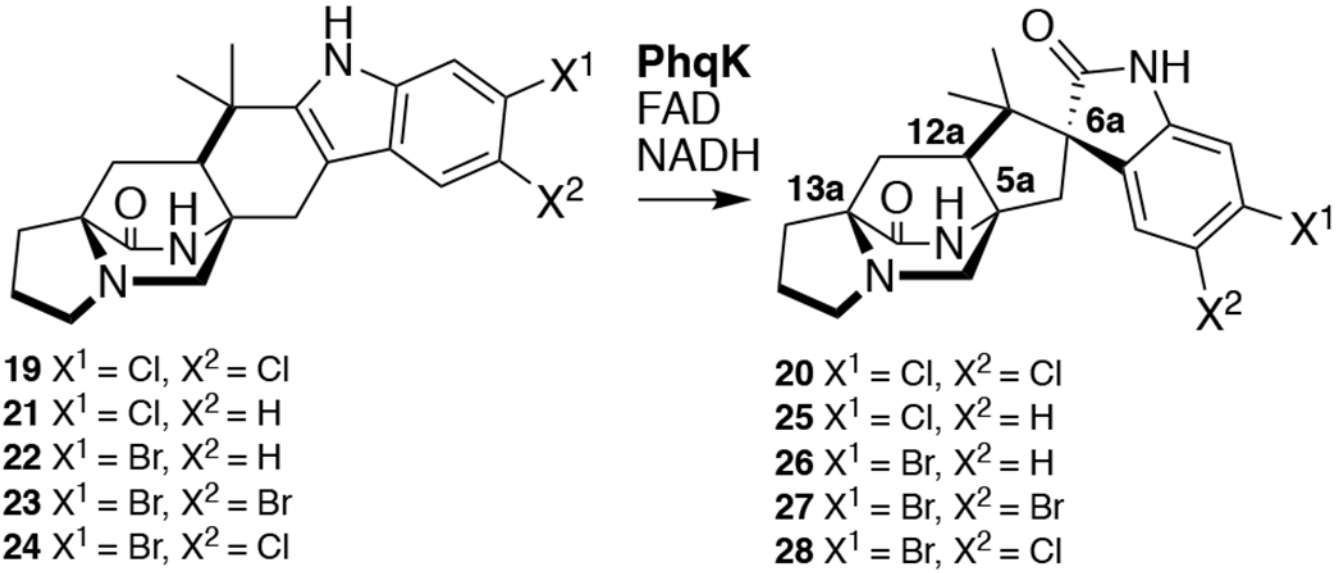

19 X^1 = Cl, X^2 = Cl
21 X^1 = Cl, X^2 = H
22 X^1 = Br, X^2 = H
23 X^1 = Br, X^2 = Br
24 X^1 = Br, X^2 = Cl

20 X^1 = Cl, X^2 = Cl
25 X^1 = Cl, X^2 = H
26 X^1 = Br, X^2 = H
27 X^1 = Br, X^2 = Br
28 X^1 = Br, X^2 = Cl

Figure 2.
Spirocyclization of malbrancheamides.

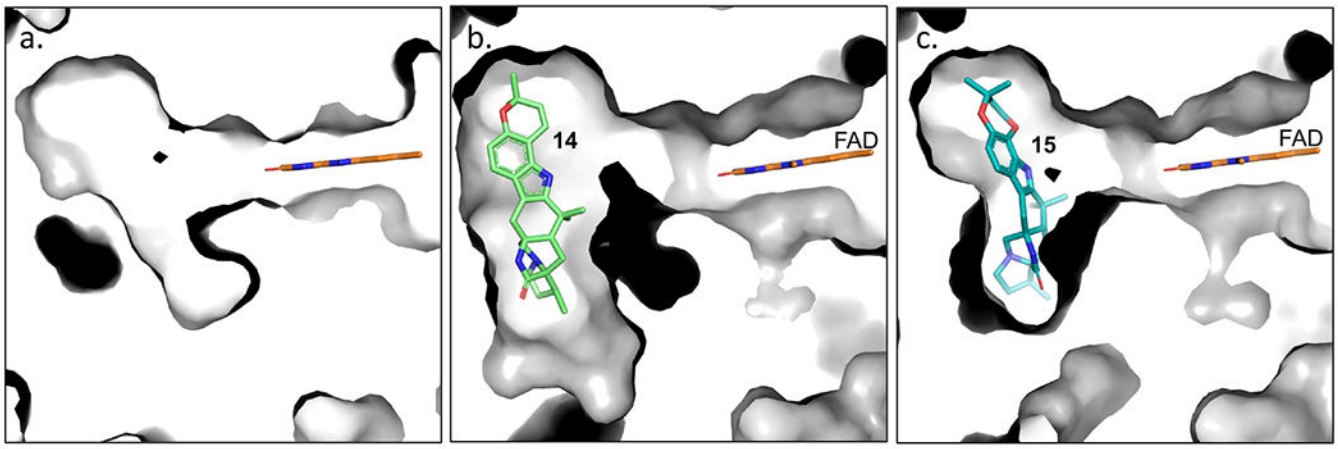

Figure 3.

Changes in the active site pocket from no ligand (a.), to accommodate substrates paraherquamide K (**14**) (b.), and L (**15**) (c.).

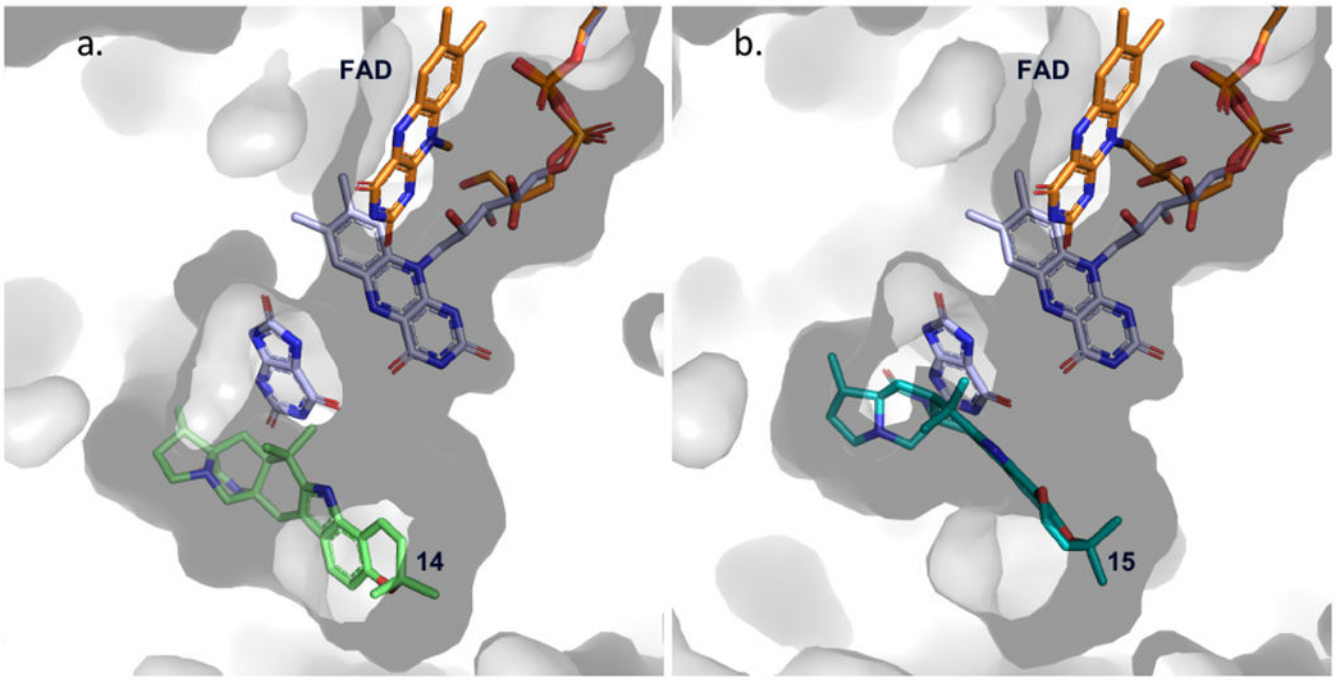

Figure 4.

Modeled cofactor dynamics in PhqK. Flavin dynamics were modeled from HpxO crystal structure (FAD and substrate in lavender) (PDB: 3rp7) to depict the “in” conformation of the flavin relative to the substrate position. The surface representation of PhqK is shown along with the substrate and FAD from the PhqK structure (orange). Substrates **14** (a.) and **15** (b.) are shown in green and teal.

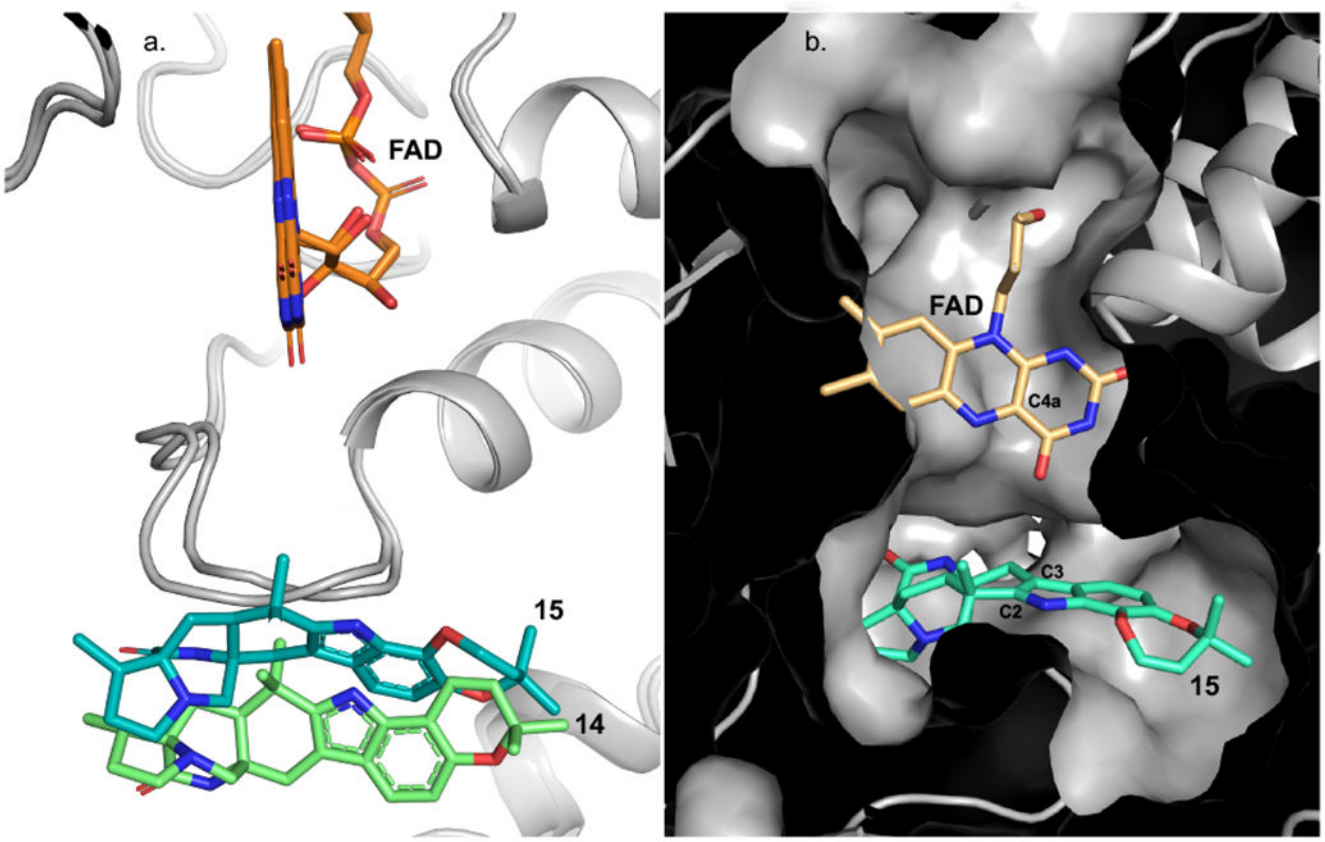

Figure 5.

(a.) Overlay of PhqK cocrystal structures. The structures are complexed with **14** (green) and **15** (teal). (b.) The "in" FAD cofactor was modeled from the HpxO structure (PDB: 3rp7) into the PhqK cocrystal structure with **15**, where the FAD-C4a is perfectly aligned to perform the epoxidation of the indole C2=C3.

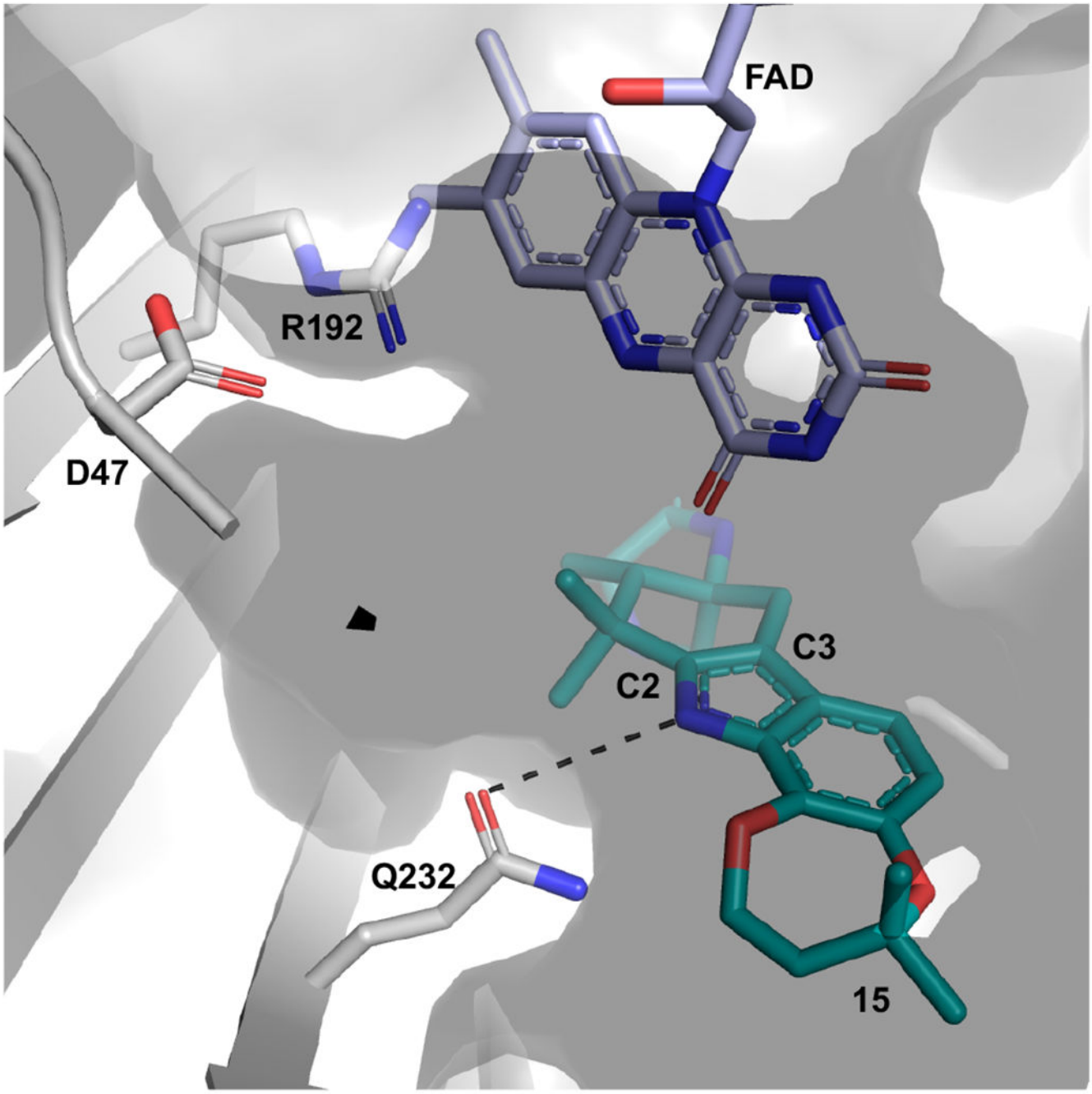

Figure 6.

Essential amino acids in PhqK active site. Cocrystal structure of PhqK with paraherquamide L (**15**) displaying the active site residues that are pertinent to the activity. The FAD is modeled in the “in” orientation.

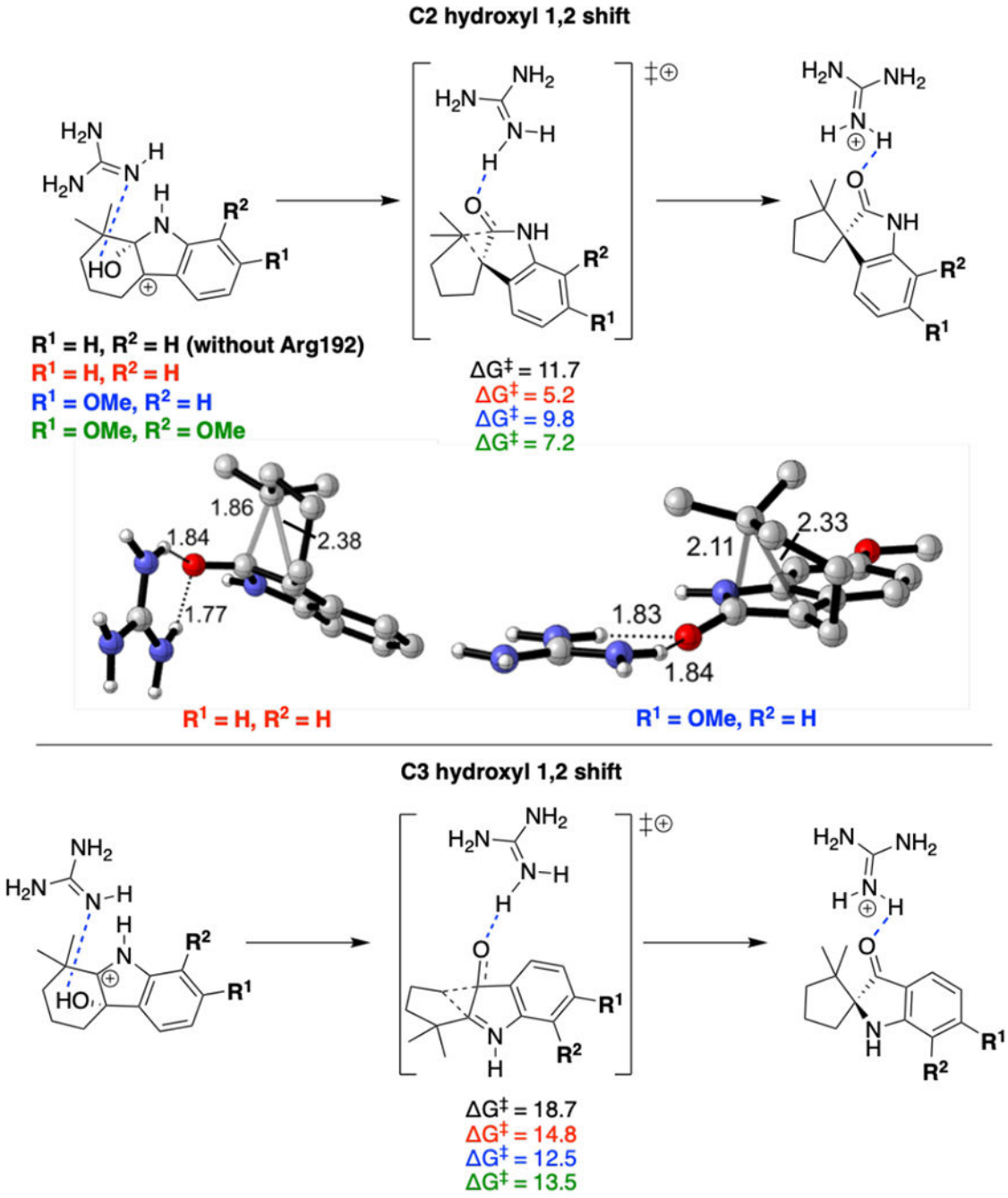

Figure 7.

General acid catalyzed transition states for 1,2 shift on C2 hydroxyl carbocation and C3 hydroxyl carbocation on a paraherquamide model system. Various indole substituents are modeled (red, blue, green) as compared to a model without general acid (black). Energies are given in kcal/mol and distances in Å.

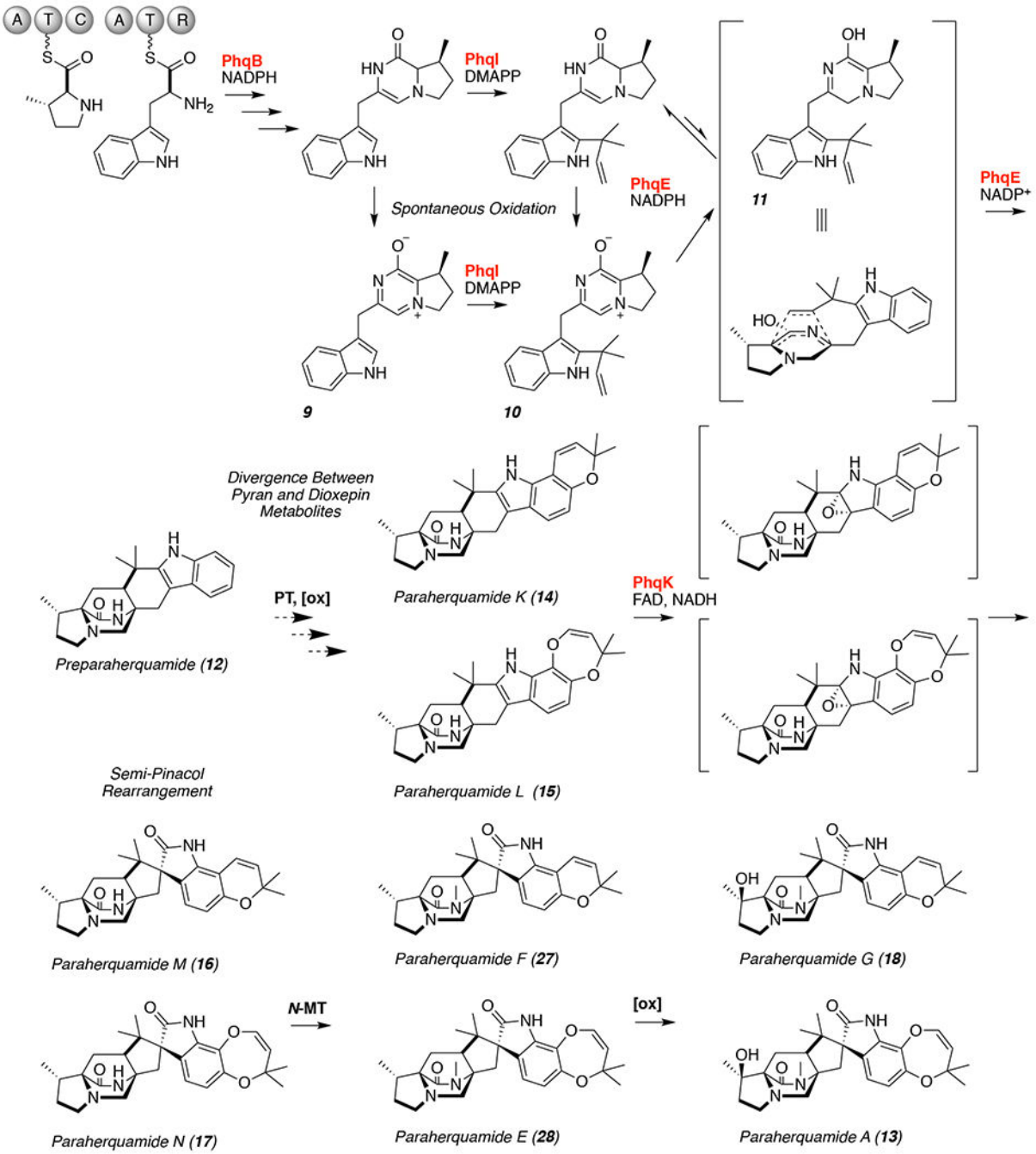

Scheme 1.

Proposed paraherquamide A (13) and G (18) biosynthetic pathways. The functions of enzymes highlighted in red have been confirmed.[11]

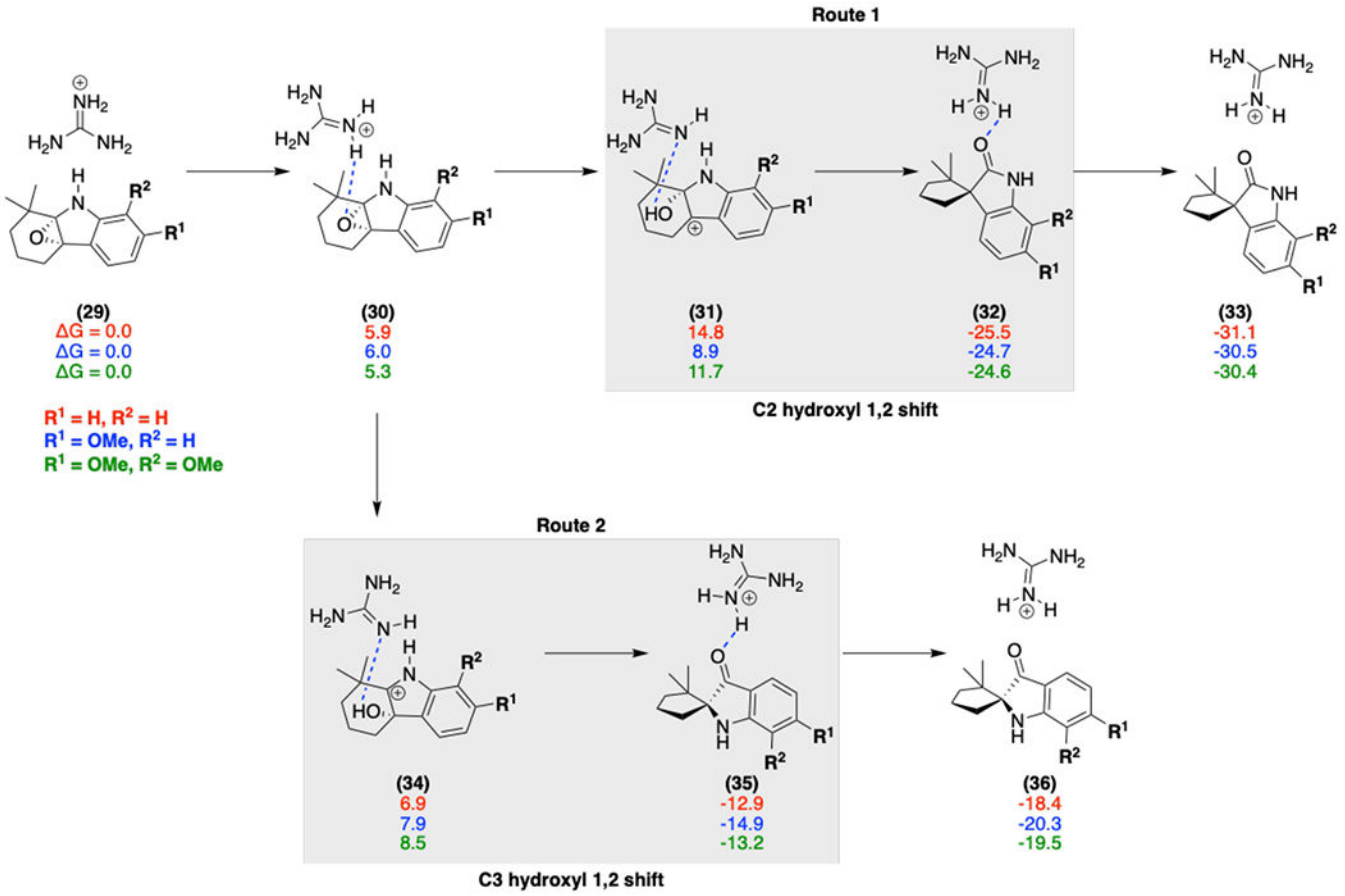

Scheme 2.

Free energies (calculated at the M06-2X/6-311++G(d,p)-ECFPCM(water)//M06-2X/6-31G(d)-IEFPCM (water) level) for various models (red, blue, green) with the Arg192 general acid (modeled by a guanidinium moiety) catalyzed epoxide ring-opening mechanism; initial protonation of the epoxide leads to ring opening to form a hydroxy cation (31 and 34), and deprotonation accompanies the 1,2 shift to generate the final spirocycle product.